International Journal of GEOMATE, Oct., 2019 Vol.17, Issue 62, pp. 77 - 83
ISSN: 2186-2982 (P), 2186-2990 (O), Japan, DOI: https://doi.org/10.21660/2019.62.4828
Special Issue on Science, Engineering & Environment

FLOW INVESTIGATIONS WITHIN A CONCENTRIC CYLINDERS OF GAS SENSOR MODULE FOR I.C. ENGINES

* Tatsuya Kawaguchi, Yoona Jeong, Takushi Saito and Isao Satoh

Tokyo Institute of Technology, Japan

*Corresponding Author, Received: 05 Jan. 2019, Revised: 02 Feb. 2019, Accepted: 25 Feb. 2019

ABSTRACT: For the global warming issues such as the reduction of greenhouse gas emissions, the exhaust gas from the internal combustion engines must be strictly controlled and purified by means of the catalytic convertor. The present investigation deal with the optical visualization of the flow field around the Zirconium sensors that is protected with concentric double cylinders with opening apertures. The commercial gas sensor modules were used for the monitoring of the Oxygen concentration before and after the catalytic convertor in passenger vehicles. In the experiment, a transparent acrylic model was used in conjunction with the particle image velocimetry as the velocimetry. The experimental result demonstrated that the magnitude of velocity in the vicinity of the sensor rod was significantly lower than that of the external main flow. The higher velocity fluctuation through the opening apertures contributes to the better mass transfer between the inside and outside of the protectors and enhances the response of the sensing module.

Keywords: Flow visualization, Gas sensor, Internal flow, Mixing process, Particle image velocimetry

1. INTRODUCTION

Regulation specifications of greenhouse gas emission and fuel economy standards for passenger vehicles and trucks were significantly progressed more than a decade. Therefore the drastic reduction of the oxidizing gases, as well as the small particles in the exhaust gas from the I.C. engine, have been required. Although only a few countries had introduced mandatory greenhouse gas emission and/or fuel economy standards, many countries including the European Union have announced their intention to introduce the greenhouse gas emission standards. Consequently, further improvement of gas emission sensing, monitoring and controlling for the internal combustion engine of automobiles, marine engines and power plants have been desired. Not only the reduction of the particulate matter but also the control of such emission gas as CO_2, NO_2 and SO_2 were required that enable to improve total efficiency of the aforementioned thermal systems[1].

In the recent engine system, multiple gas sensor modules are equipped that measure the various kinds of gas species such as O_2 concentration difference between catalysts, which is feed backed to the engine control unit. Figure 1 illustrates the exhaust gas flow system after the combustor for passenger vehicles. In order to determine the catalytic convertor working properly, the multiple gas sensor module was applied. Figure 2 shows the photograph of the actual engine compartment of the vehicle. The sensor module of the exhaust gas sensor module for commercial vehicles consists of the cylindrical rod of Zirconium dioxide as a sensor core with heater and dual stainless cylindrical shrouds with multiple openings or apertures. The shrouds prevent the sensor core from the direct exposure to the high-temperature exhaust gas as well as the liquid droplet. Since the operation temperature of the sensor rod is significantly high, the penetration of the particulate objects and liquids to the sensor core must be avoided. Therefore, most of all commercial sensor module employs the protectors with off-axis multiple apertures in both concentric shrouds. Figure 3 depicts the sectional image of the head section of the sensor module. As shown in the figure, Zirconia sensor rod is located at the axis of the multiple cylinder. External air flow penetrates through the multiple apertures and finally reached to the heated sensor element. O_2 concentration difference between inner- and outer sensor element surfaces produces the electrical voltage difference between both surfaces.

Since the concentration fluctuation of the exhaust gas could be detected by the electrode surface, which is protected by the concentric shrouds, the time lag between concentration

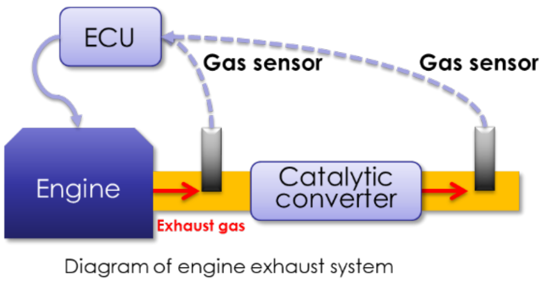

Fig. 1 Gas sensor alignment at the exhaust system of the combustor.

fluctuation and electrical output of the sensor module is presented in terms of the alignment of the opening apertures. Moreover, the frequency response of the sensor module is decreased due to the aforementioned delay effects.

In order to clarify the characteristics of the sensor and to improve the overall performance of the gas sensor modules, the detailed behavior of the fluid flow around the sensor core, as well as the flow between multiple concentric protectors, must be investigated. Especially, the flow convection through the multiple opening apertures is the significant factor for the evaluation of the mass transportation between sensor core and external flow of protector. In the present study, we focused on the investigation of the fluid flow behavior in the protectors by means of the optical visualization technique in terms of the geometrical alignments of the opening apertures or air slit in the multiple protectors.

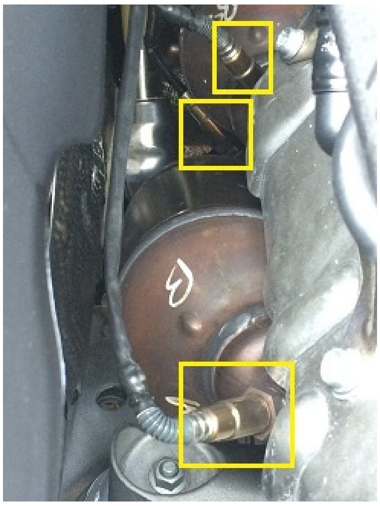

Fig. 2 Gas sensors attached to the exhaust system for the actual passenger vehicle. Three rectangular in the figure indicates the sensor module. As the head of the module is plugged into a pipe, neither sensor element nor protectors are visible

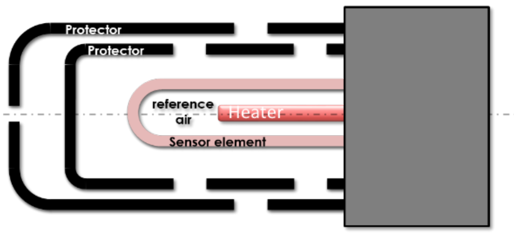

Fig. 3 Details of the internal structure of the gas sensor. The sensor module consists on the heated zirconia sensor element and concentric dual stainless protectors with multiple opening apertures. The offset alignment of the apertures prevent the droplet and particles from impacting onto the sensor surface.

2. FLOW VISUALIZATION BY PARTICLE IMAGE VELOCIMETRY

For the industrial applications, gas or liquid flow around the cylinder or rectangular obstacles is one of the most important flow fields. Especially the flow analysis around a finite cylinder is the important external flow, therefore numerous experimental and numerical investigations were reported that deal with the detailed behavior of the flow around the rectangular or cylindrical objects [2-4]. However, not so many investigations of the flow structure by using the hollow cylinder or cylindrical object with by-pass channels was reported [5,6]. In the present study, we focused on the fluid flow visualization within the gas sensor module for the automobile applications.

Figure 4 illustrated the experimental set up for the optical flow visualization used in the following experiments. Particle image velocimetry (PIV) [7,8] was employed as a velocity measurement method. For the measurement target, a transparent analogous model of which geometry is proportional to the actual sensor module was employed [9,10]. As the preliminary experiments, detailed air flow behavior in the concentric protectors was investigated under the steady flow. The model was installed in a rectangular transparent channel with honeycomb and electrical fans. Both width and height of the channel was 240 mm, length of the channel was 910 mm. In the present study, velocity distribution at the channel entrance was assumed to be homogeneous. Continuous-wave Nd:YAG laser was used in conjunction with the high-speed CMOS camera. Output power and wavelength of the laser light source was 2 W and 532 nm respectively. Maximum frame rate of the camera was 800 fps.

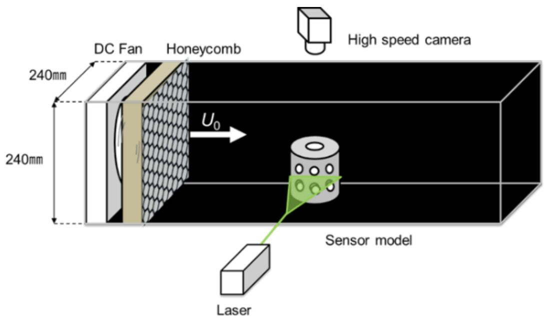

Fig. 4 Experimental rig for the flow visualization by means of the particle image velocimetry.

Table 1. Comparison between experimental parameters between actual exhaust gas flow and present experiment.

	Actual gas sensor	Model experiment
Material	Stainless steel (SUS304)	Acrylic resin
Protector diameter,	~10 mm	100 mm
Temperature	850 ~ 1050 K	300 K
Kinematic viscosity ν (10^{-6} m^2/s)	120	12
Max. velocity	~100 m/s	1.3 m/s
Gas components	• CO_2 - 13% •Water vapor - 11% •N2 - 76%	Air
Reynolds number	8300	

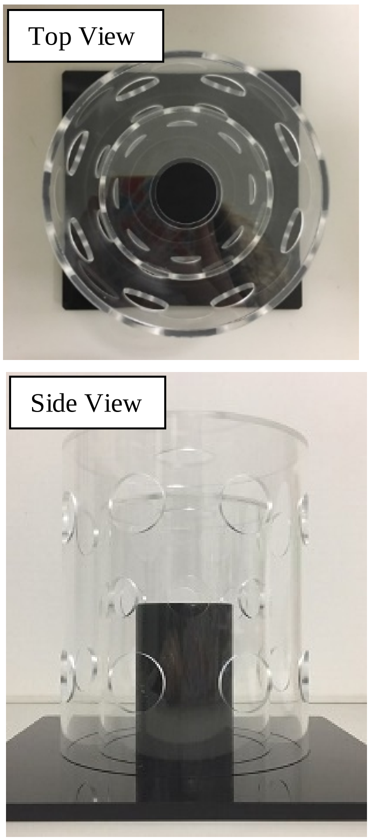

Fig. 5 Transparent acrylic model for the flow visualization consisted of outer and inner hollow cylinders (protectors), inner solid cylinder (sensor rod). Diameters of cylinders were 100, 70 and 40 mm, heights were 123, 98, and 61 mm, respectively. Both protectors have multiple opening apertures.

Pixel dimension was 1920x1080 that affected the resultant frame rate due to the limitation of the data transfer bandwidth of the USB3 digital connection between CMOS camera head and personal computer. For the velocity vector map calculation, standard recursive cross correlation with the sub-pixel Gaussian fitting estimation was employed in which the coarse velocity vector map was firstly obtained by using the frequency-domain cross correlation that is followed by the fine computation of the cross correlation coefficients for the determination of the subpixel displacement of particle images.

Geometrical shape of the transparent acrylic model was determined by noting the Reynolds number of the actual flow field. Table 1 compares the representative parameters of the actual sensor system and present experiment. Kinematic viscosity of high temperature exhaust gas is ten times as higher as the working fluid at room temperature and atmospheric pressure. Two photographs in figure 5 shows the top view and side view of the concentric cylinders used in the experiments. The model was divided into triple concentric cylinders, which consisted of outer protector, inner protector and sensor core rod. In this experiment, the sensor is replaced by the plastic solid cylinder instead of the zirconium rod with a heater. External diameter of the outer protector, inner protector and the core were 100 mm, 70 mm and 40 mm respectively. Since the size of cylinders used in the experiment was ten times as larger as the actual sensor module, resultant velocity magnitude of main flow in the experimental rig was on the order of 1 m/s. As shown in figure 6, eight circular apertures were prepared by 45 deg for the inner cylindrical protectors. On the inner protector surface, in-line eight opening aperture were aligned. External protector has dual-line eight apertures as well. On the center-top of the cylinders, the other aperture was prepared. The diameter of each opening aperture was 20 mm. Figure 6 is an example of the colored captured image around the test section illuminated with the monochromatic laser light source. The parameter, θ, represents the absolute angle from the direction of upstream, i.e. the main flow is coming from the direction of $\theta = 0$. As tracer particles, smoke from an incense stick was used that has the better traceability to the airflow as well as the better maintainability of the experimental rig. Mean diameter of the tracer particle was a few µm. It was confirmed that the relaxation time of the solid

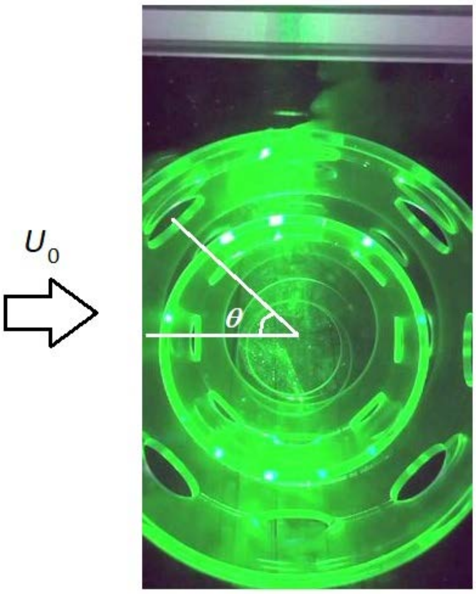

Fig. 6 Snapshot of the experimental model that is consisted of the triple cylinders. Tracer particles were illuminated by using the continuous-wave (CW) Nd:YAG laser sheet. Angular position, θ, is defined as the angle between main flow direction and aperture location.

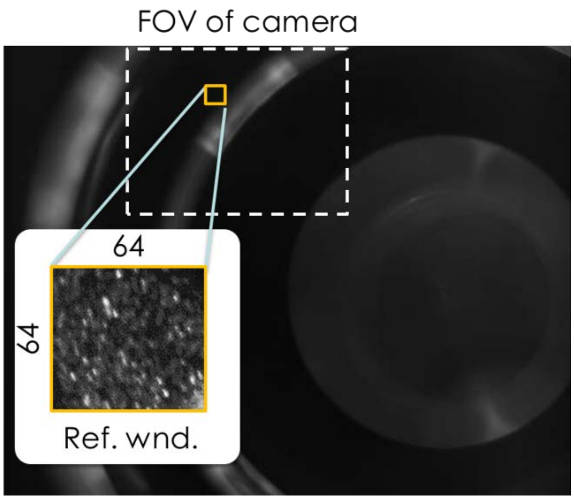

Fig.7 Field of view (FOV) of the CMOS sensor in the experiment. Pixel dimension of the reference window for the PIV interrogation was 64 pixel times 64 pixel.

tracer particles was sufficiently smaller than that of the air flow.

3. RESULT AND DISCUSSION

Figure 7 depicts the example of the output from the CMOS camera and corresponding area of view. Due to the maximum spatial resolution of the optics as well as the limitation of the pixel number of the

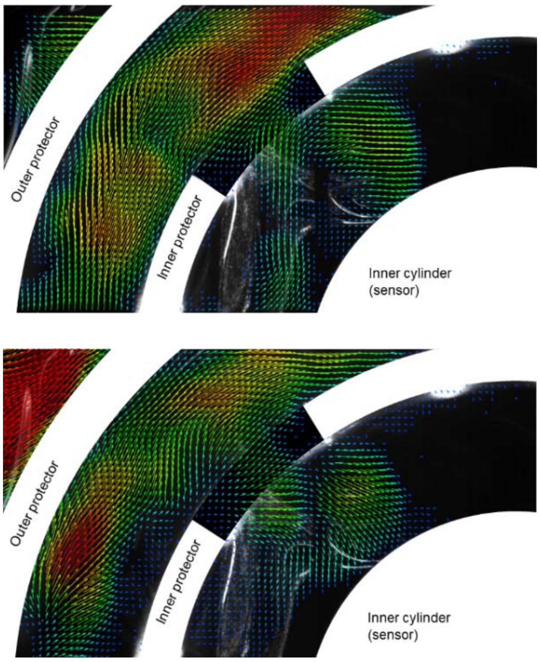

Fig. 8 Examples of the instantaneous velocity vector map through the opening aperture of the inner protector. Both vector map were obtained with the identical conditions such as flow rate, protector alignment.

image sensor, the entire imaging system was traversed and captured image sequence one by one. The dashed line in the figure represents the field of view of the imaging system. Figure 8 shows the instantaneous velocity vector map in the vicinity of the opening aperture of the inner protector at the difference instance. Mean velocity of the main flow was 0.15 m/s. From the visualization results of the velocity vector map around the sensor core rod, the magnitude of the velocity at the sensor core surface was drastically decreased due to the geometrical structure in the cavity and the multiple apertures. Although the external main flow was steady, the velocity within the protectors was significantly modulated due to the complicated geometry of the opening apertures, i.e., the fluid behavior within the protector is not steady and the flow direction, as well as the magnitude of velocities, fluctuated. To clarify the effects of the aperture positions, the location of the opening apertures and the orientation of each protector were varied as a parameter.

From the instantaneous velocity vector map obtained by the velocimetry, the spatial mean velocity through an aperture, which is equivalent to the volume flux through the aperture, was derived. By obtaining the local velocity vector at the opening surface,

$$\mathbf{U} = (u,v) \tag{1}$$

As well as the normal vector of the opening aperture

$$\mathbf{n} = (-dy,\, dx) \tag{2}$$

As shown in figure 9, the volume flow rate through the apertures was calculated by using the following formula.

$$\bar{U} = \frac{\dot{Q}}{A} = \frac{1}{A}\int \mathbf{U}\cdot\mathbf{n}\, dA \tag{3}$$

Angular offset of both outer and inner protectors were varied as (0, 0), (0, 22.5), (22.5, 0) and (22.5, 22.5) in degree respectively. By the comparison of the aperture phase differences, the effects of the offset angle of the opening apertures were evaluated. The relative offset of apertures between outer and inner protectors was due to the design of the sensor element. In contrast, the absolute value of the apertures reflects the impinging angle of the main flow to the sensor module. The latter could be varied due to the attached angle of the sensor and fluid flow behavior such as secondary flow in exhaust pipe systems. Both effects were considered at the following analyses.

Figure 10 compares the spatially averaged velocity transition through the opening apertures with the angles of (0, 0) deg. Velocity transition under the other three alignment was obtained with the same flow configuration. The negative value of the normal velocity component indicates the

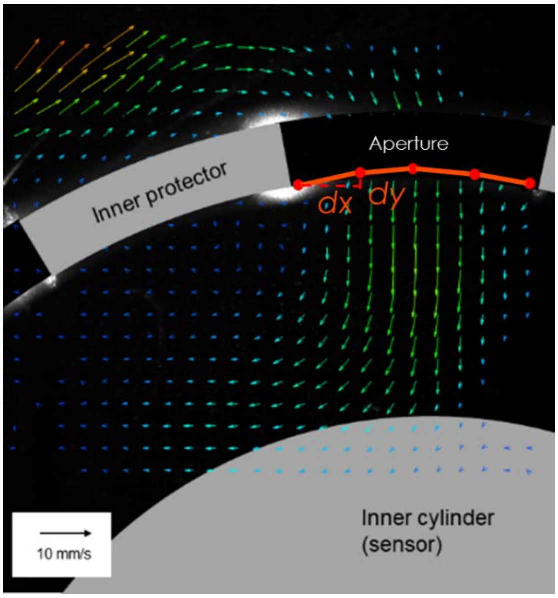

Fig. 9 Spatial average of the vector for the estimation of the volume flow rate through the apertures.

incoming volume flux toward the sensor core. In contrast, the positive velocity indicates the outgoing flow to the external main flow. Under the configuration, air flow through the upwind aperture,

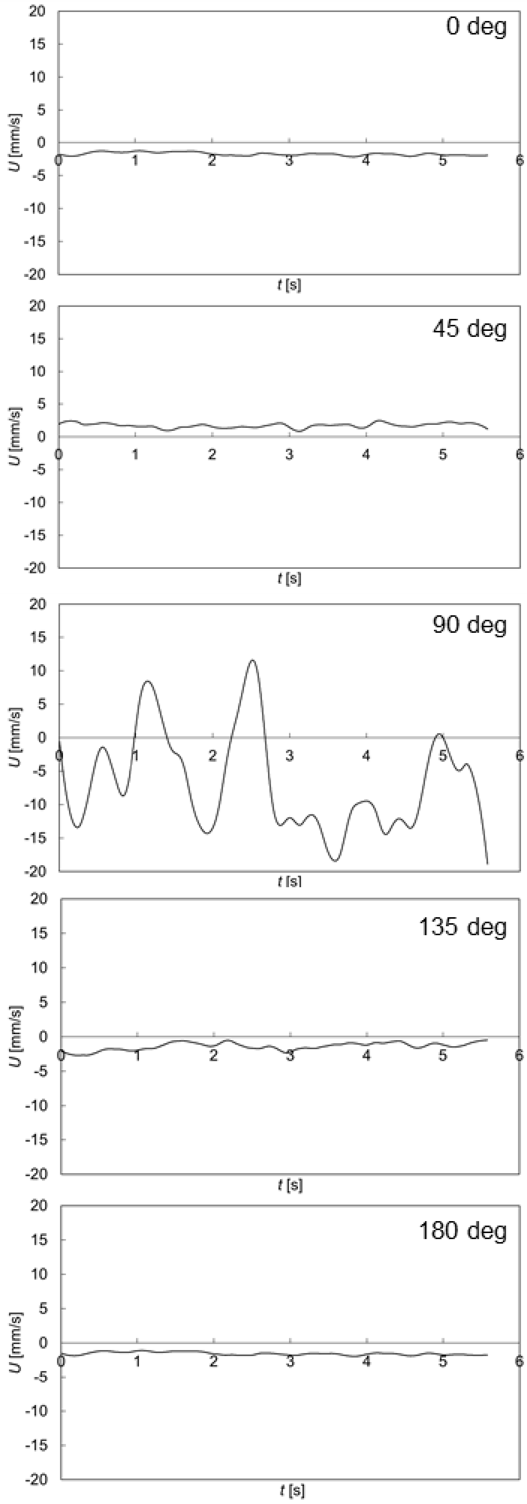

Fig. 10 Comparison between mean velocity magnitudes through the opening aperture. Each angle value in the figure represents the angular position of the opening apertures of (0,0) deg.

which was located at $\theta = 0$ deg, was quite stable and the magnitude of the cross-sectional mean velocity was -2.0 mm/s approximately. Since the opening aperture is present at the upward stagnation point at $\theta = 0$ deg in which the relative pressure is higher than that of the other apertures, incoming flow through the corresponding aperture was observed. In contrast, the fluid velocity through the side aperture at $\theta = 90$ deg was significantly fluctuated. Mean velocity through the side aperture was -6.7 mm/s, therefore the volume flux through the side aperture was 2.1 cm^3/s of incoming direction. Comparison of the velocity fluctuations at the different alignment of the protectors of (22.5, 22.5) deg resulted that both mean velocities during the period were 2.5 mm/s and 6.3 mm/s, volume fluxes were 0.79 cm^3/s and 2.0 cm^3/s respectively. The comparison of the angular alignment of protectors demonstrated that the outgoing flow occurs even at the upstream aperture.

In order to compare and clarify the aforementioned flow pattern, angular distribution of mean velocity and velocity fluctuation of each aperture position in terms of the offset angles of the protectors were summarized in figure 11 and figure 12 respectively.. The comparison of the mean velocity through the apertures demonstrated that the incoming and outgoing flow appeared at the downward and upward apertures respectively. The velocity distribution indicated that the overall flow direction within the inner protector was inverted to the external main flow. Consequently, the direction of volume flux through the sensor core is opposed to the external mainstream. In contrast to the lower and stable mean velocity distribution around the core rod, the significant velocity fluctuations were observed in the vicinity of the aperture located on the side of the inner protector that enhanced the convective mass transfer.

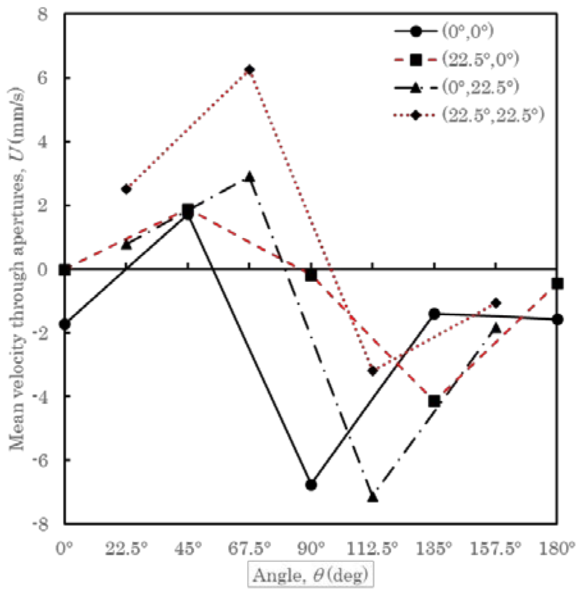

Fig. 11 Spatial-temporal mean velocity through the opening apertures. Offset angles of both protectors were varied

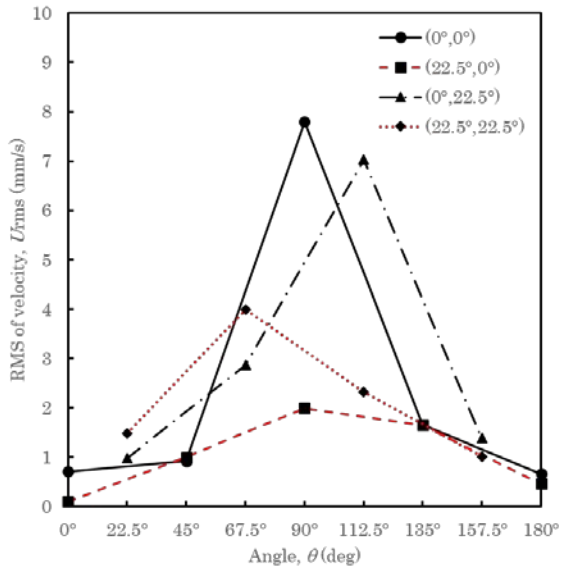

Fig. 12 Angular distribution of velocity fluctuation in terms of the angular alignments of the opening apertures of both protectors.

4. CONCLUSIONS

In order to understand the flow behavior in a gas sensor module, flow in dual protectors with multiple apertures was investigated. The flow field in the concentric triple cylinders was measured by means of particle image velocimetry (PIV). A transparent acrylic model was designed and used for optical visualization. The geometrical shape was determined by considering the Reynolds number matching with the actual gas sensor for a passenger vehicle. The quantitative visualization resulted that the flow direction within the inner protector was inverted to the external main flow. The velocity magnitude of the internal flow is significantly lower than that of the main flow. The throughput of the concentration modulation around the sensor could be enhanced by the velocity fluctuation around the side apertures that contribute to the quick response of the entire sensor module. Under the present configuration, sensor response was maximized with (0, 0) deg alignment of both protectors' apertures.

5. REFERENCES

[1] Yamada T, Hayakawa N, Kami Y and Kawai T, Universal Air-Fuel Ratio Heated Exhaust Gas Oxygen Sensor and Further Applications, SAE 920234, 1992.

[2] Wang H F and Zhou Y, The finite-length

square cylinder near wake, J. Fld. Mech., Vol. 638, pp. 453-490, 2009.

[3] Rostamy N, Sumner D, Bergstrom D J and Bugg, J D, Local flow field of a surface-mounted finite circular cylinder, J. Fld and Structures, Vol. 34, pp. 105-122, 2012.

[4] Pattenden R J, Turnock S R and Zhang X, Measurements of the flow over a low-aspect-ratio cylinder mounted on a ground plane, Exp. Fld., Vol. 39, pp. 10-21, 2005.

[5] Rinoshika H, Rinoshika A and Fujimoto S, Passive control on flow structure around a wall-mounted low aspect ratio circular cylinder by using an inclined hole, J. Fld. Sci. and Technol., Vol., 12, No. 1, JFST0006, 2017.

[6] Rinoshika H, Rinoshika A and Fujimoto S, Visualization of a finite wall-mounted cylinder wake controlled by a horizontal or inclined hole, J Visualization. https:// doi.org/10.1007/ s12650-012-6, 2018.

[7] Adrian R J, Particle-Imaging Techniques for Experimental Fluid Mechanics, Annu. Rev. Fld Mech., Vol. 23, pp. 261-304, 1991

[8] Prasad A K, Stereoscopic particle image velocimetry. Exp. Fluids 29, 2, pp. 103-116

[9] Kawaguchi T, Jeong Y N, Saito T and Satoh I, Flow visualization in the cylindrical shrouds with apertures of the Oxygen sensor for the exhaust gas, Proc. 18th Int. Symp. Flow Visual., Zurich, Switzerland, 2018

[10] Kawaguchi T, Jeong Y N, Saito T and Satoh I, Flow investigations within a concentric cylinders of gas sensor module for I.C. engines, Proc. 4th Int. Conf. on Sci., Eng & Env (SEE), Nagoya, Japan, 2018.